Elimination and strengthening of glycinergic/GABAergic connections during tonotopic map formation

Gunsoo Kim and Karl Kandler

Department of Neurobiology, University of Pittsburgh School of Medicine, 3500 Terrace Street, Pittsburgh, Pennsylvania 15261, USA
Correspondence should be addressed to K.K. (kkarl@pitt.edu)

Published online 10 February 2003; doi:10.1038/nn1015

Synapse elimination and strengthening are central mechanisms for the developmental organization of excitatory neuronal networks. Little is known, however, about whether these processes are also involved in establishing precise inhibitory circuits. We examined the development of functional connectivity before hearing onset in rats in the tonotopically organized, glycinergic pathway from the medial nucleus of the trapezoid body (MNTB) to the lateral superior olive (LSO), which is part of the mammalian sound localization system. We found that LSO neurons became functionally disconnected from ~75% of their initial inputs, resulting in a two-fold sharpening of functional topography. This was accompanied by a 12-fold increase in the synaptic conductance generated by maintained individual inputs. Functional elimination of MNTB–LSO synapses was restricted to the period when these glycinergic/GABAergic synapses are excitatory. These results provide new insights into the mechanisms by which precisely organized inhibitory circuits are established during development.

Elimination and strengthening of excitatory synaptic connections by spontaneous or experience-evoked neuronal activity are critical steps in the developmental organization and fine-tuning of neuronal circuits[1–7]. However, direct evidence for the involvement of synapse elimination/strengthening in the formation of organized inhibitory circuits has remained largely elusive. Most cellular mechanisms and models thought to mediate synaptic plasticity and reorganization depend on the depolarizing and spike-eliciting effects of excitatory synapses, effects that generally are not associated with inhibitory synapses.

Compared with the clear organization that is present in topographically organized excitatory pathways, the detailed anatomical organization of most inhibitory circuits is obscure. In most brain areas, inhibition is generated by local inhibitory networks, which are composed of anatomically and functionally distinct local interneurons. This organization represents a major obstacle for specific experimental manipulations and the developmental analysis of inhibitory circuits. Thus, despite accumulating evidence for plasticity and developmental changes in global levels of inhibition[8–10] and its further influence on excitatory plasticity[11–13], interpretation of these changes at the level of specific inhibitory connections has been difficult.

To date, perhaps the best evidence in support of spatial fine-tuning of inhibitory networks comes from studies of the developing auditory system[14–16]. In mammals, evidence from two sound localization circuits has demonstrated the presence of specific reorganization of inhibitory connectivity. In the medial superior olive of gerbils, anatomical analysis shows an activity-dependent cellular redistribution of glycinergic synapses, a process that is thought to be important for processing interaural time differences in this species[15]. In the lateral superior olive (LSO), pruning of immature glycinergic/GABAergic axon terminals and refinement of LSO dendrites support the hypothesis that elimination of inhibitory synapses sharpens inhibitory connectivity[17,18]. It remains unclear, however, whether and to what degree these anatomical changes reflect the reorganization of an operative inhibitory network rather than the structural elimination of exuberant (and perhaps non-functional) immature synaptic contacts or axonal processes.

Here we investigated the emergence of a precisely organized inhibitory circuit by analyzing functional connectivity and synaptic properties of MNTB–LSO connections in developing rats before hearing onset. Neurons in the MNTB are glycinergic in adult animals and glycinergic/GABAergic during development[16,19] and give rise to a purely inhibitory and precisely tonotopically organized pathway to the LSO[18,20] (**Fig. 1a**). The MNTB–LSO pathway carries auditory information from the contralateral cochlea. The frequency-specific alignment of this inhibitory pathway with excitatory inputs from the ipsilateral cochlea provides the neuronal basis for encoding the interaural intensity differences used for sound localization[21]. Our results indicate that the establishment of the functional topography of the MNTB–LSO pathway is accomplished by extensive, but specific, elimination of functional glycinergic/GABAergic synapses and by an increase in the synaptic conductance elicited by maintained connections. Notably, functional elimination of MNTB–LSO connections takes place while these connections are excitatory, lending support to the hypothesis that the transient excitatory action of immature inhibitory synapses is an important mechanism for organizing the development of inhibitory circuits.

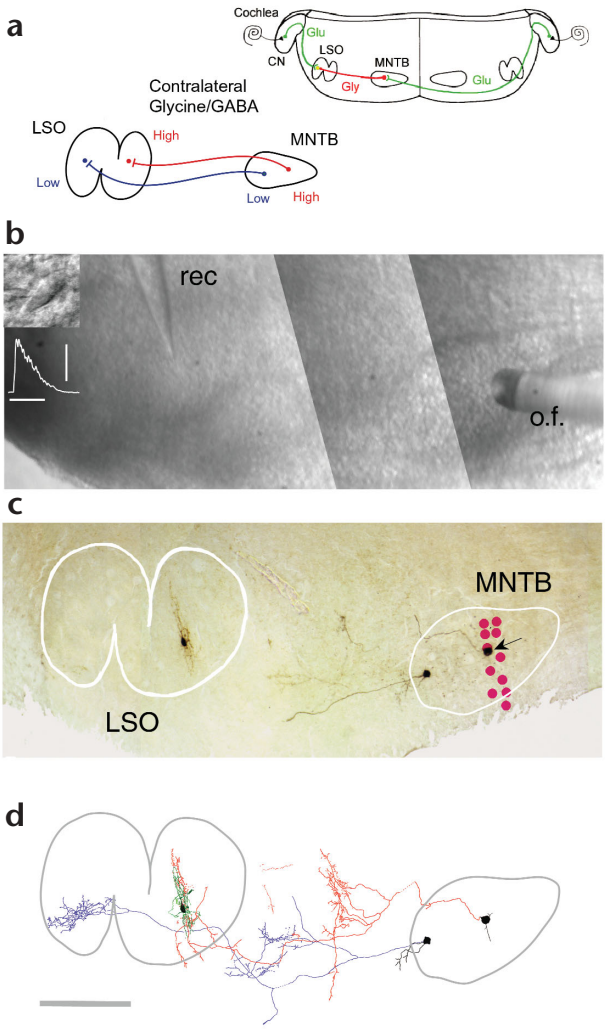

Fig. 1. Focal photolysis of caged glutamate in auditory brainstem slices reveals functional GABAergic/glycinergic connections in the MNTB–LSO pathway. (**a**) Illustration of afferent connections to the lateral superior olive (LSO). In adult animals, both inputs converge on single LSO neurons in a precise tonotopic manner. The tonotopic organization of the MNTB–LSO pathway is shown in the enlargement. (**b**) Montage of video images taken during a mapping experiment. The recording electrode (rec) is positioned in the medial limb of the LSO, and the movable optical fiber (o.f.) is positioned above the MNTB. Photo inset shows an IR-image of a typical LSO neuron with elongated cell body and two emerging primary dendrites. The trace inset shows a synaptic response elicited by uncaging glutamate in the MNTB of a P11 animal (flash duration 100 ms, indicated by horizontal bar). Vertical scale bar, 10 mV. (**c**) The location and morphology of the recorded LSO neuron in (**b**) is revealed by biocytin staining. Red circles in MNTB mark uncaging sites from which PSPs could be elicited in the LSO neuron. For clarity, non-responding sites in and around the MNTB are excluded. Two MNTB neurons were filled with biocytin: one within the input map (arrow) and the other outside the input map. (**d**) Camera-lucida drawings of biocytin-filled neurons. Notice the close overlap of axonal terminals from the MNTB neuron located inside the input map (red) with the recorded LSO neuron (green). Additional MNTB axon collaterals are visible in several other auditory nuclei. Scale bar, 200 μm.

Results

Whole-cell patch-clamp recordings were obtained from visually identified principal neurons in the LSO in brainstem slices (**Fig. 1**)[17,22]. To determine the spatial distribution of presynaptic MNTB neurons, 80–120 discrete locations spaced ~50 μm apart were stimulated in the MNTB using focal photolysis of caged glutamate (**Fig. 1b** and **c**)[23]. Detection of weak glycinergic/GABAergic connections was enhanced by increasing the driving force for chloride to about –50 mV while blocking postsynaptic action potentials (5 mM QX314 in the pipette solution). Under these conditions, stimulation of glycinergic/GABAergic MNTB neurons evoked depolarizing postsynaptic potentials (PSPs, **Fig. 1b**, inset) or inward postsynaptic currents (PSCs). Consistent with the glycinergic/GABAergic nature of the immature MNTB–LSO pathway[19,24], synaptic responses were abolished by bicuculline (10 μM) and strychnine (10 μM) (data not shown). At all ages, the reversal potential of MNTB-evoked responses was about –20 mV, close to the calculated value of the chloride reversal potential.

To confirm that functional MNTB–LSO connectivity, as revealed by uncaging glutamate, indeed reveals direct anatomical MNTB–LSO projections, MNTB neurons were filled with biocytin, and their axonal termination pattern in the LSO was determined ($n = 10$; **Fig. 1c** and **d**). MNTB neurons located inside the functionally connected area formed axon terminals that closely intermingled with the dendritic tree of the postsynaptic LSO neuron. In contrast, axon terminals of MNTB neurons residing in nonresponsive areas were completely segregated from the dendritic trees of recorded LSO neurons (**Fig. 1d**, blue). Together, these results support the suitability of our approach to reveal functional MNTB–LSO connectivity.

Spatial refinement of MNTB–LSO connectivity

To examine the development of the spatial organization of functional MNTB–LSO connectivity, we determined MNTB–LSO input maps to individual LSO neurons in rats at postnatal days 1 (P1) to P14. In all neonatal animals, PSPs could be elicited from a large number of MNTB sites that gave rise to wide, dorsoventrally oriented input areas (30,579 ± 1,739 μm^2, $n = 8$, P1–P4; **Figs. 2a** and **b** and **3a**). On average, these input areas covered about 36% of the corresponding MNTB cross sectional areas (35.6 ± 2.2%, $n = 8$; **Fig. 3a–c**). Input maps were always contiguous, however, suggesting that at birth, MNTB–LSO connections already show some degree of topographical organization[18,25].

MNTB–LSO input areas from animals around hearing onset were markedly smaller than those from neonatal animals (10,988 ± 1,668 μm^2, $n = 15$, P11–P14, $P < 0.001$, Student's t-test; **Figs. 2c** and **d** and **3a**), and gave rise to narrow, generally dorsoventrally oriented maps that on average covered about 8% of the corresponding MNTB areas (8.3 ± 1.3%, $n = 15$; P11–P14, $P < 0.001$, Student's t-test; **Fig. 3a–c**). Thus, during the first two postnatal weeks, normalized MNTB input areas decreased by about 75%. Elongated input maps observed around the time of hearing onset were oriented perpendicular to the mediolateral frequency axis in the MNTB[26] and thus followed isofrequency contours (**Fig. 2c** and **d**).

To quantify the sharpening of MNTB–LSO input maps in terms of refinement along the tonotopic axis, we measured the width of maps along the mediolateral MNTB axis (input width). During the first two postnatal weeks, absolute and MNTB-normalized input width decreased by about 50% (absolute width: P1–P4, 113.7 ± 5.2 μm, $n = 8$; P11–P14: 62.6 ± 3.8 μm, $n = 15$; $P < 0.001$, Student's t-test; normalized width: P1–P4, 27.9%; P11–P14, 12.4%; **Fig. 3d–f**). Thus, spatial refinement of the MNTB–LSO pathway resulted in a two-fold sharpening of the topographic organization in the frequency domain, rather than a general reduction of con-

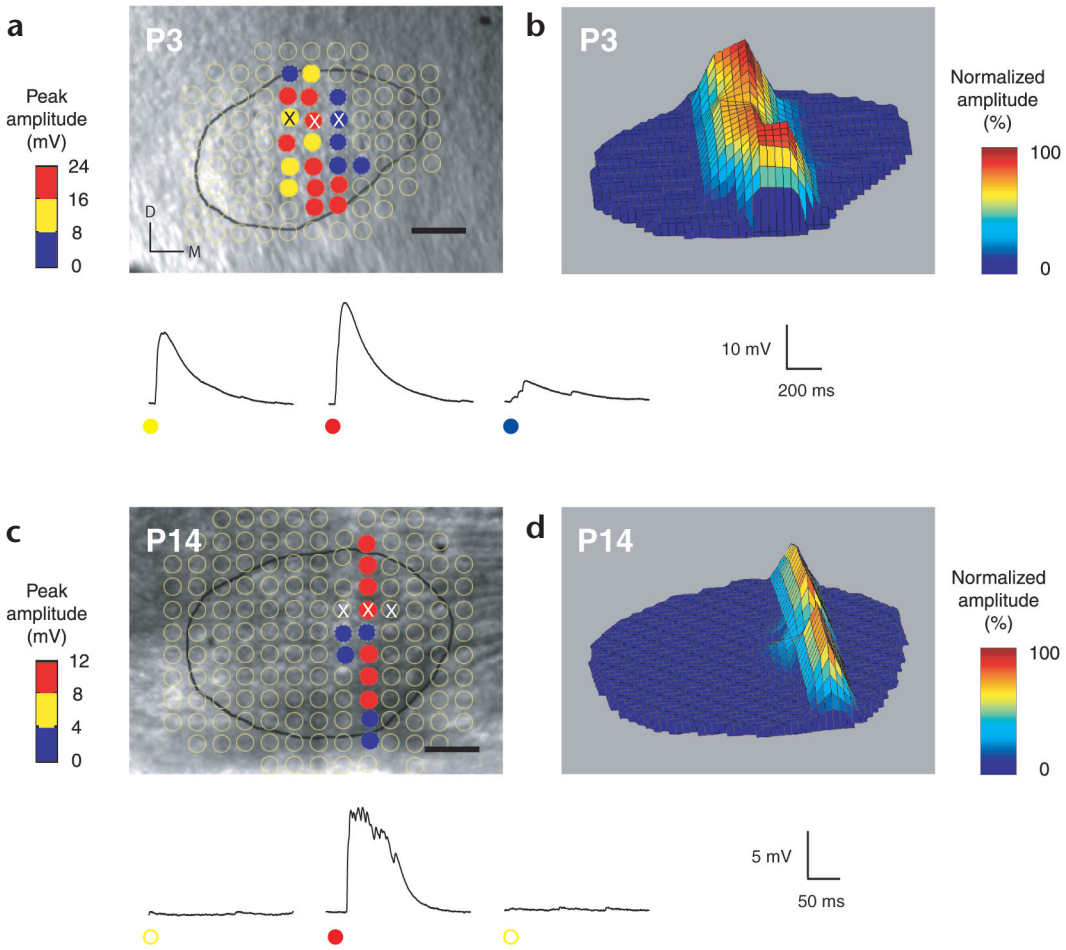

Fig. 2. MNTB–LSO input maps from a P3 (**a**, **b**) and a P14 rat (**c**, **d**). (**a**) Location of unresponsive (open circles) and responsive (colored circles) stimulation sites are overlaid onto a video picture of the MNTB (outlined in black). Responsive areas are color-coded according to peak amplitudes of postsynaptic LSO responses. Examples of synaptic responses elicited from three locations (marked with x) are illustrated in the lower traces. (**b**) Interpolated 3-D plot of input areas. The size of the MNTB is scaled to match the size at P14 (**d**). (**c**, **d**) MNTB–LSO input map from a P14 rat. Scale bars (**a**, **c**) are 100 μm.

nectivity over the entire map. This frequency-specific sharpening of functional MNTB–LSO connectivity occurred mainly between P3 and P8 and was essentially complete at P9, about 3–5 days before hearing onset (**Fig. 3b** and **e**).

These conclusions depend on two premises: first, that the efficacy of uncaging glutamate remains constant from P1 to P14, and second, that uncaging glutamate at younger ages does not activate polysynaptic pathways from the MNTB to the LSO. Myelination of afferent and efferent fibers in the MNTB, however, could increase scattering of ultraviolet (UV) light and thus affect the amount of free glutamate uncaged in the tissue. In addition, maturation of glutamate receptors and membrane properties of MNTB neurons[27] may alter the responses of MNTB neurons to a given concentration of uncaged glutamate. To address these issues, we determined the effective resolution of glutamate uncaging in the MNTB of neonatal (P2–P3) and older animals (P12–P13) by directly recording responses of MNTB neurons to uncaging glutamate nearby. UV flashes aimed directly at the cell body readily elicited action potentials at all ages (**Fig. 4a**). In neonates, responses consisted of only one or two slow action potentials, whereas trains of fast action potentials occurred in older animals. The bursts of action potentials in older MNTB neurons should ease the detection of functional connections, tending to increase, rather to decrease, the size of input maps (See also **Supplementary Figs. 1** and **2**).

Uncaging glutamate at some distance from the cell body produced subthreshold depolarizations or no responses (**Fig. 4a**). Because only spiking MNTB neurons generate synaptic responses in LSO neurons, we determined uncaging resolution as the maximum distance from the cell body at which UV flashes elicited spikes. Along the mediolateral axis, this distance was about 25 μm and was equivalent in neonatal and older animals (P2–P3, 26.5 ± 2.0 μm, $n = 8$; P11–P13, 23.8 ± 1.5 μm, $n = 6$; $P > 0.3$, Student's t-test; **Fig. 4b**). Along the dorsoventral axis, however, the distance was approximately twice as large in neonatal animals as in older animals (P2–P3, 48.4 ± 11.2 μm, $n = 8$; P11–P13, 21.4 ± 1.4 μm, $n = 6$; $P < 0.05$, Student's t-test). The decrease of spike-eliciting distance along the dorsoventral direction may reflect increasing myelination of horizontal fibers, which would restrict diffusion of glutamate in the dorsoventral direction, or it may reflect developmental changes in the physiological or morphological properties of dendrites of MNTB neurons.

The age-dependent change in resolution along the dorsoventral axis could produce an overestimation of input areas in younger

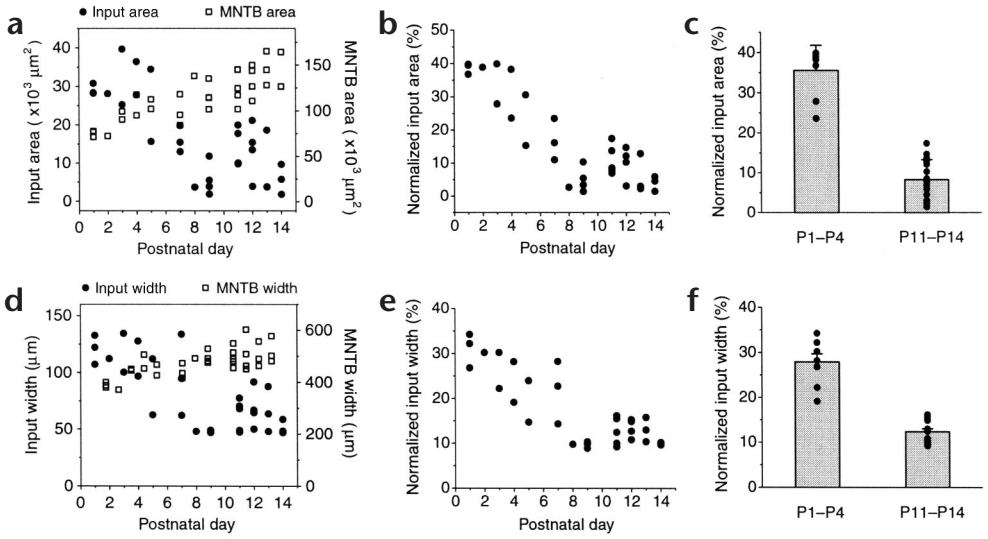

Fig. 3. Age-dependent decrease in the size and width of MTNB–LSO input maps. (**a**–**c**) Changes in input areas. (**a**) MNTB–LSO input areas (filled circles) and MNTB cross-sectional areas (open squares) as a function of age. (**b**) Input areas normalized to the corresponding MNTB cross-sectional area. (**c**) Normalized input areas in newborn and 2-week-old animals (P1–P4, $n = 8$; P11–P14, $n = 15$; $P < 0.001$; Student's t-test). (**d**–**f**) Extent of input maps along the tonotopic axis in the MNTB (input width). (**d**) Absolute input width (filled circles) and mediolateral extension of the MNTB (open squares) as a function of age. (**e**) Input width normalized to corresponding MNTB width. (**f**) Normalized input width in newborn and 2-week-old animals (P1–P4, $n = 8$; P11–P14, $n = 15$; $P < 0.001$; Student's t-test).

animals because of the possible 'filling in' of small MNTB areas that in fact are not connected to the recorded LSO neuron. However, because uncaging efficacy along the mediolateral axis remained stable, our measurements of input width are not affected by maturation of the MNTB. Using the 50% decrease in input width (**Figs. 2** and **3d–f**) as a conservative estimate, we conclude that individual LSO neurons become functionally disconnected from at least 50% of their initial presynaptic MNTB partners.

Developmental changes in stimulus–response functions

A parsimonious explanation for the observed topographic sharpening is that it reflects the selective elimination of topographically exuberant connections. Alternatively, at these early developmental stages, topographic reorganization of MNTB–LSO connectivity might be caused by concentrating initially dispersed MNTB neurons with similar 'tonotopic identities' into LSO 'isofrequency stripes'. In addition, our mapping studies cannot address the question of whether elimination of inappropriate connections is counterbalanced by the formation of new connections from topographically appropriate areas.

To address these issues, we analyzed synaptic responses to electrical stimulation of MNTB inputs while blocking potential contamination of postsynaptic currents by glutamatergic inputs[19,24] with kynurenic acid (1 mM). The maximum synaptic peak current at saturating stimulation intensities (see Methods) increased more than threefold during the first two postnatal weeks (P1–P5, 1.4 ± 0.33 nA, $n = 16$; P9–P14, 4.5 ± 0.54 nA, $n = 18$; $P < 0.01$, Student's t-test; **Fig. 5a**). These results indicate that the elimination of MNTB–LSO connections is either outweighed by the formation of new connections or counteracted by an increase in the synaptic conductance elicited by maintained connections.

To distinguish between these possibilities, we estimated the number of MNTB axons that converge on individual LSO neurons by gradually increasing electrical stimulus intensities. Small increments in stimulus intensity gradually recruit more fibers, and the number of discrete response amplitude increments should provide a lower estimate of the number of converging fibers[1,4,28]. In all LSO neurons recorded from neonatal animals (P1–P5, $n = 16$), PSC peak amplitudes smoothly increased as a function of stimulus intensity (**Fig. 5b**). This is consistent with the idea that at this early age, LSO neurons are innervated by a large number

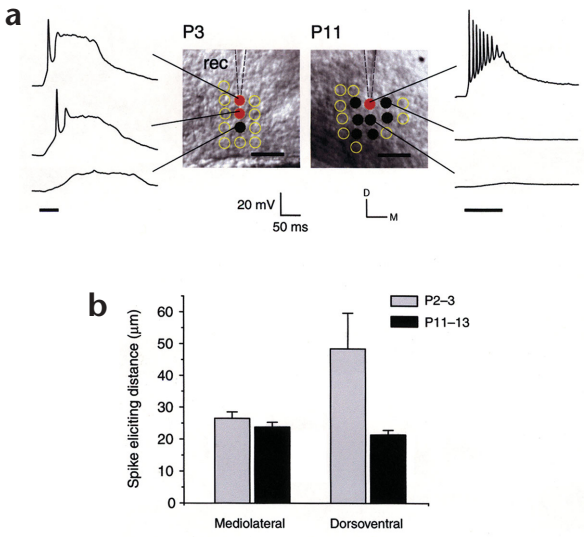

Fig. 4. Spatial resolution of uncaging glutamate during MNTB maturation. (**a**) Responses of a P3 and a P11 MNTB neuron to photolysis of caged glutamate. At both ages, stimulation sites that elicit action potentials (filled red circles) are restricted to the immediate vicinity of the cell body at the tip of the recording electrode (rec). Stimulation sites at greater distances elicit subthreshold membrane depolarizations (black filled circles) or no responses (open yellow circles). D, dorsal; M, medial. Scale bar, 100 µm. (**b**) Maximal dorsoventral and mediolateral spike-eliciting distance (P2–P3, $n = 8$; P11–P13, $n = 6$).

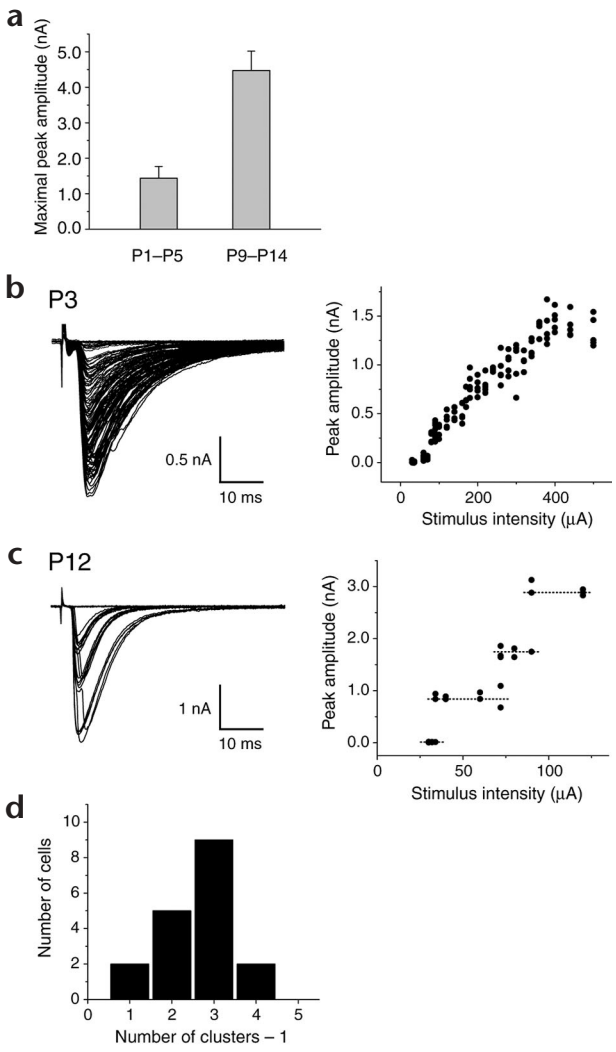

Fig. 5. Number of inputs to LSO neurons declines postnatally. (**a**) Maximal synaptic peak currents in P1–P5 (n = 16) and P9–P14 animals (n = 18). (**b**) Stimulus–response relationship in a P3 neuron. Left, superposition of synaptic currents elicited by electrical stimulation of the MNTB axon bundle with intensities between 30 μA and 500 μA. Right, plot of synaptic current peak amplitudes versus stimulus intensities reveals a smooth stimulus–response relation. (**c**) Stimulus-response curve relationship in a P12 neuron. Left, superposition of synaptic currents elicited by electrical stimulation with intensities between 30 μA and 120 μA. Right, plot of synaptic current peak amplitudes versus stimulus intensities reveals three pronounced increments. Dotted lines indicate medians for each step as derived from cluster analysis. Recording solution contained the L-type calcium channel antagonist D600 (1 mM). (**d**) Histogram of number of response steps (number of non-zero clusters) identified in 18 neurons from P9–P14 animals.

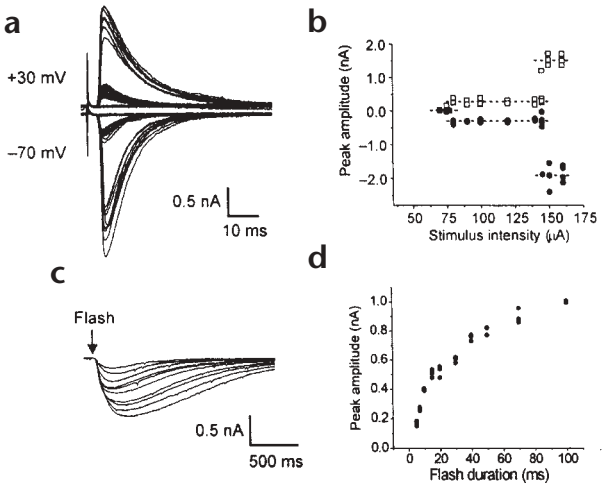

Fig. 6. Response steps are not caused by activation of postsynaptic voltage-gated ion channels. (**a**, **b**) Response steps occur during voltage-inactivation of postsynaptic voltage-gated ion channels. (**a**) Synaptic currents in a P11 LSO neuron alternately held at –70 mV (inward currents) or +30 mV (outward currents). Membrane potential was changed to +30 mV 1.2 s before electrical stimulation. (**b**) Corresponding stimulus–response curve. Notice the presence of response steps around 80 and 150 μA at each holding potential. Dotted lines indicate medians for each cluster. (**c**, **d**) Activation of postsynaptic GABA receptors by rapid photolysis of caged GABA produces smooth stimulus–response curves. (**c**) Overlaid postsynaptic currents elicited by gradually increasing UV flash durations from 5 ms to 100 ms. (**d**) Peak responses vary smoothly as a function of flash duration. V_{hold} = –70 mV.

of MNTB axons, each of which contributes only a small fraction to the total postsynaptic current. In contrast, in all neurons recorded from older animals (P9–P14, n = 18), PSC amplitudes increased in discrete steps in response to increasing stimulus intensities (**Fig. 5c**). The beginning and end of different response steps usually overlapped, consistent with the stochastic nature of fiber recruitment at threshold intensities. The number of amplitude steps, as determined by cluster analysis (Methods), varied between 1 and 4 (average 2.6 ± 0.2, n = 18), with 50% of neurons showing three response steps. These results are consistent with the idea that around the time of hearing onset, LSO neurons are contacted by only a few MNTB fibers, each of which generates large PSCs. It should be noted, however, that the number of converging fibers probably represents a lower bound due to the severance of some fibers during slice preparation. Nevertheless, these results support the idea that functional elimination of MNTB–LSO connections during topographic sharpening is paralleled by an increase in the synaptic conductances generated by single fibers.

During the first two postnatal weeks, LSO neurons undergo maturation both in dendritic complexity and in active and passive membrane properties[17,29]. This could complicate the interpretation of step-like responses in older LSO neurons if these steps resulted from the activation of dendritic voltage-gated currents that escaped voltage-clamp. Several observations, however, argue against this possibility. First, discontinuous stimulus–response curves were readily observed when Na^+-channels and L-type Ca^{2+}-channels were blocked by the inclusion of QX314 (5 mM) and the L-type calcium channel antagonist D600 (0.1 mM) in the pipette solution (QX314, n = 18; QX314 + D600, n = 9; example shown **Fig. 5c**), and there was no difference in the number of steps recorded in neurons with QX314 + D600 (2.7 ± 0.3, n = 9) versus QX314 alone (2.6 ± 0.3, n = 9). Second, discontinuous stimulus–response functions were also obtained when voltage-gated membrane currents were inactivated by holding neurons at positive membrane potentials (+30 mV, n = 4; **Fig. 6a** and **b**) and all steps observed at –70 mV were also observed at +30 mV (2.5 ± 0.3 steps for both holding potentials, n = 4). Finally, direct dendritic application of GABA by focal photolysis of caged GABA (BC204, 200 μM) produced smooth stimulus–response curves despite the fact that the same neurons produced step-like response

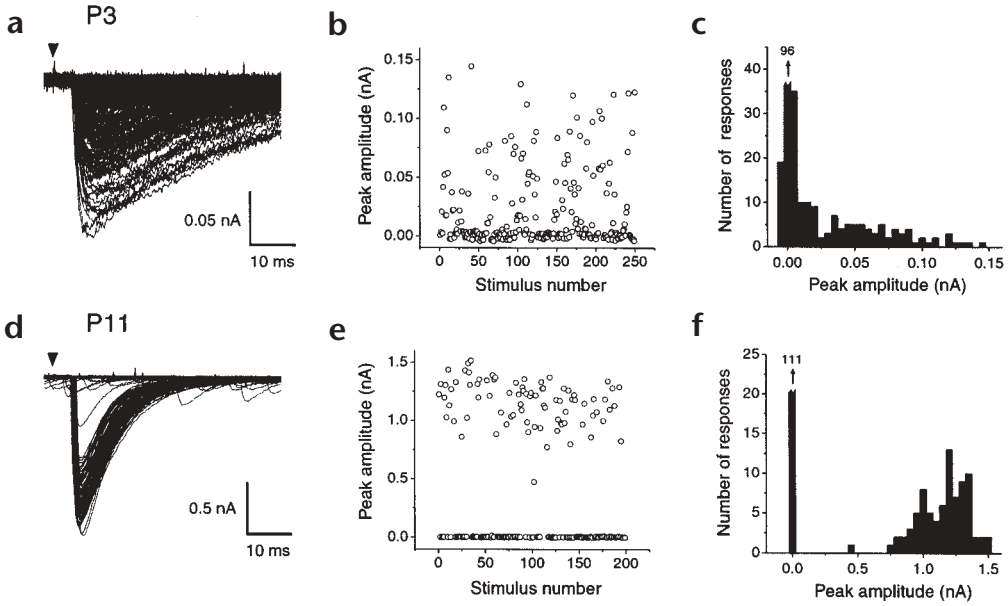

Fig. 7. Minimal stimulation of MNTB inputs. (**a**–**c**) Synaptic responses in a P3 neuron. (**a**) Superposition of 250 consecutive currents. (**b**) Plot of peak amplitudes and (**c**) amplitude histogram of responses shown in (**a**). (**d**–**f**) Synaptic responses in a P11 neuron. Note different scales of abscissa in (**c**) and (**f**). For both neurons, the stimulus frequency was 0.067 Hz. Failure rates were about 60%, and their frequency bars are truncated in (**c**) and (**f**). Arrowheads indicate stimulus.

increments with synaptic stimulation ($n = 2$; **Fig. 6c** and **d**). We therefore conclude that the step-like response increments observed at older ages reflect activation of additional fibers rather than activation of postsynaptic active membrane conductances.

Developmental increase of single-fiber inputs

Quantitative measurements of convergence based on stimulus–response increments critically depend on the ratio of increment size to variability, such that cluster analysis may not detect weak contributions. In young animals, all inputs were small relative to single-fiber response variability, making it impossible to count distinct inputs with cluster analysis.

We thus estimated the number of converging fibers in neonatal animals by estimating the strength of single MNTB fibers using minimal stimulation, an approach based on the idea that with stimulus intensities at threshold, only a single fiber is likely to be recruited[30]. In all neurons from neonatal animals (P1–P5), minimal stimulation produced responses with variable amplitude (14–140 pA, $n = 19$ cells; **Figs. 7a–c** and **8a**), even when stimulus intensities were decreased to result in failure rates >70% ($n = 3$). A likely explanation for these variable amplitudes is that responses are elicited by individual inputs that form multiple synapses on the recorded LSO neuron. Minimal stimulation responses in neurons from older animals (P9–P14) were markedly larger (30 pA to 2,400 pA, $n = 23$ cells; **Figs. 7d–f** and **8b**). In addition, there was also a pronounced decrease in the decay times of synaptic currents, most likely reflecting the decrease in the GABAergic component over this developmental period[19,31]. The average single-fiber response was 57 ± 10 pA in P1–P5 animals and 719 ± 134 pA in P9–P14 animals ($P < 0.01$; Student's t-test). Thus, synaptic currents generated by single MNTB fibers increased more than 12-fold during the first two postnatal weeks. There was no correlation between rise times and amplitudes of single-fiber currents in older animals (10%–90% rise times, 0.71–1.47 ms; amplitudes, 30.6 pA to 2.4 nA; $n = 23$; $r = -0.08$), arguing against the possibility that the increase in synaptic currents was primarily due to selective somatodendritic relocalization of inhibitory synapses, as occurs in developing MSO neurons in gerbils[15].

Results from the electrical stimulation experiments allowed us to estimate quantitative changes in the MNTB:LSO conver-

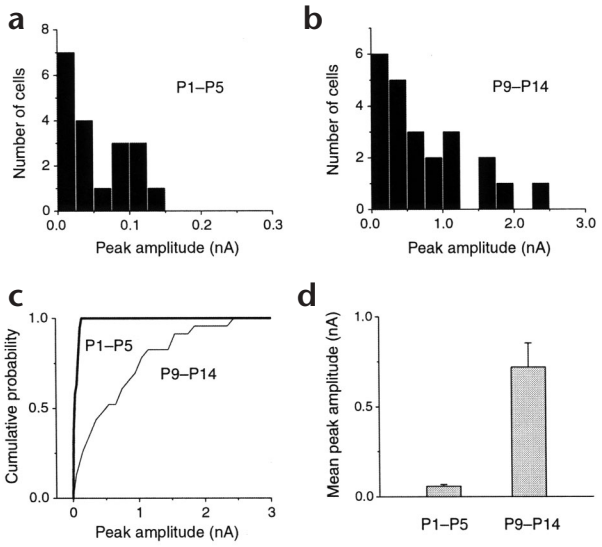

Fig. 8. Age-dependent changes in single-fiber strength. (**a**) Amplitude histogram of average single-fiber responses in neonatal animals (P1–P5, $n = 19$). (**b**) Amplitude histogram of average single fiber responses in older animals (P9–P14, $n = 23$). Note different scale of abscissa between (**a**) and (**b**). (**c**) Cumulative amplitude histograms for the two age groups ($P < 0.001$, Kolmogorov-Smirnov test). (**d**) Mean amplitudes of single-fiber responses in P1–P5 and P9–P14 animals ($P < 0.01$; Student's t-test).

gence ratio over the period of spatial refinement. In P1–P5 animals, total synaptic currents generated by all MNTB axons converging on individual LSO neurons were 1.4 nA (**Fig. 5a**), and the average single-fiber response was 57 pA (**Fig. 8d**). Thus, we estimated MNTB:LSO convergence ratio in neonatal animals to be ~25:1. In P9–P14 animals, total synaptic currents generated by all converging MNTB inputs was 4.5 nA, and the average single-fiber response was 719 pA, indicating that the estimated MNTB:LSO convergence ratio around hearing onset is ~6:1. These convergence ratios represent conservative estimates because some MNTB–LSO connections most likely were severed during slice preparation and because single-fiber responses are biased toward higher amplitudes by exclusion of all failures (Methods). In addition, because of the variable responses encountered in neonatal animals, some of the larger responses at this age could reflect the stimulation of more than one fiber, which would result in a bias toward higher fiber conductances and possible underestimation of convergence ratios at this age. Nevertheless, the reduction in the convergence ratio from 25:1 to 6:1 closely matches the ~75% reduction in the size of MNTB–LSO input maps. The difference between the 6:1 ratio obtained from minimal stimulation and the 3:1 ratio obtained from cluster analysis suggests that around hearing onset, LSO neurons on average receive inputs from about three MNTB fibers that generate large synaptic currents and three MNTB axons that generate very small synaptic currents (included in **Fig. 8b**).

Discussion

In the present study, we applied functional mapping with caged glutamate and electrical stimulation techniques to the developing MNTB–LSO pathway to shed more light on the events by which an inhibitory circuit in the mammalian brain becomes organized during normal development. Our results indicate that specific elimination of functional connections and an increase in synaptic conductances elicited by the remaining connections are two prominent mechanisms involved in the formation of a tonotopic, inhibitory map. Synapse elimination is extensive and rapid, as individual LSO neurons become functionally disconnected from ~75% of their initial presynaptic MNTB partners in only 5–6 days. Concomitant with this elimination process, synaptic currents generated by maintained connections increase ~12-fold.

A surprising finding of our mapping studies is that functional elimination of MNTB–LSO connections occurs primarily during the first postnatal week (**Fig. 3a** and **e**), which is before the onset of hearing (around P12–P14 in rats)[32]. This contrasts with previous anatomical data showing that tonotopic refinement in the MNTB–LSO pathway takes place primarily during the third postnatal week, which is after hearing onset[17,18]. The 50% functional sharpening along the tonotopic axis that we observed before P8 (**Fig. 3f**) exceeds the degree of anatomical refinement that takes place after hearing onset (~35% sharpening of boutonal spread along tonotopic axis[18]). Thus, precise tonotopy of the MNTB–LSO pathway apparently emerges via two distinct processes: functional refinement during the first postnatal week and structural refinement during the third postnatal week. Delays between functional refinement and structural refinement have been observed previously in the developing neuromuscular junction[33] and visual cortex[34]. In these excitatory systems, changes in synaptic transmission are followed by axonal rearrangement in only one or two days, whereas in the glycinergic/GABAergic MNTB–LSO pathway, synaptic silencing and axonal pruning are separated by about one week. As a consequence of this long delay, functional and structural refinement seems to take place during two distinct developmental periods during which the developing auditory system is in two fundamentally different physiological stages.

First, synaptic silencing takes place when glycinergic/GABAergic MNTB–LSO synapses are excitatory[35,36], whereas structural synapse elimination occurs when MNTB–LSO synapses are inhibitory. As in many other brain areas[37], glycine and GABA in the LSO gradually change from being excitatory to being inhibitory. In the LSO of rats, this transition is completed by P8, the age after which functional MNTB–LSO connectivity is stable (**Fig. 3**). Such a correlation is predicted by the hypothesis that the excitatory action of inhibitory synapses is crucial for the developmental organization of inhibitory networks[37]. Consistent with this, depolarizing MNTB–LSO synapses increase postsynaptic calcium concentration[24], which is an essential step for inducing plasticity in a variety of glycinergic and GABAergic synapses[37–39]. This scenario predicts that formation of early functional topography in the MNTB–LSO depends on spontaneous activity and perhaps synaptic competition, as is the case in a number of excitatory systems[6,40]. The fact that spontaneous activity is necessary for sustaining functional MNTB–LSO connections before hearing onset[41] and that it is a critical factor in the formation and maintenance of glycinergic and GABAergic synapses in other systems [8,10,42] is consistent with this idea. Axonal pruning of MNTB axons during the hyperpolarizing phase[18,19,35] most likely involves a different set of cellular mechanisms that is independent of depolarization-induced calcium influx[38,39].

Second, because functional elimination of MNTB–LSO synapses is essentially complete by P8, at least 4 days before hearing onset (**Fig. 3**), sound-evoked neuronal activity is not involved in the initial steps of topographic sharpening. This differs from the prevalent view, based on anatomical observations, that tonotopic sharpening of the MNTB–LSO pathway takes place primarily in the presence of sound-evoked activity[16–18]. Although alteration of normal MNTB–LSO activity levels or patterns by cochlear ablation results in less precise MNTB–LSO connectivity, it is unknown whether these effects are due to changes in spontaneous or sound-evoked activity[43]. For example, normal auditory experience may guide the structural manifestation of the functional tonotopic organization of the MNTB–LSO pathway that is present at hearing onset, or it may reactivate 'silent' MNTB–LSO connections[44] to further fine-tune LSO circuits to the changing acoustic geometry of the growing head.

The roughly 4-fold decrease in convergence ratio before hearing onset is compensated by a roughly 12-fold increase in the synaptic conductance generated by individual MNTB axons. Developmental changes in receptor subunit composition[16] or neurotransmitter phenotype[19] are unlikely to account for these changes because changes in subunit composition have relatively little effect on channel conductances, which tend to decrease rather than increase during development[45,46]. It is thus more likely that the increase in synaptic conductance reflects an increase in the number of release sites, postsynaptic receptors and/or probability of release[5,44,47]. Homeostatic synaptic scaling, a process by which the strength of synapses is regulated to counteract changes in overall neuronal activity[8,48], could provide a possible explanation for the increase in synaptic conductance during synapse elimination. However, additional mechanisms, such as age-dependent changes in the excitation set point of LSO neurons, would then be required to account for the excitation–inhibition switch. Finally, it remains to be shown how, during this excitation–inhibition switch, the pronounced increase in synaptic conductance influences postsynaptic responses to MNTB activity and integration of excitatory and inhibitory inputs in the LSO.

Our results lend strong, albeit correlative, support for the long-standing hypothesis that the seemingly paradoxical excitatory effect of immature inhibitory synapses is crucially involved in the initial establishment of early developing inhibitory networks[37]. Further detailed analysis of the developing MNTB–LSO system could uncover the cellular and molecular mechanisms guiding early specification of inhibitory circuits and their fine-tuning at later developmental stages[10,14–16,18,38,39,43].

Methods

Animals and slice preparation. All experiments used slices from neonatal rats (P1–P14; Sprague-Dawley, Charles River Laboratories, Wilmington, Massachusetts). Experimental procedures were in accordance with NIH guidelines and were approved by the IACUC at the University of Pittsburgh. Brainstem slices (300–400 μm) were prepared as previously described[24] (for details, see **Supplementary Methods**).

Electrophysiology. Whole-cell patch-clamp recordings were obtained from visualized principal-type LSO neurons identified by their bipolar morphology. Recordings were obtained from the medial part of the LSO, which corresponds to the tonotopic high-frequency region[26]. Location and morphology of neurons was confirmed by filling neurons with biocytin (0.5% in pipette solution). Mapping experiments were conducted in current-clamp. Electrodes (5–6 MΩ) were filled with solution containing 54 mM potassium gluconate, 56 mM KCl, 1 mM $MgCl_2$, 1 mM $CaCl_2$, 5 mM sodium phosphocreatine, 10 mM HEPES, 11 mM EGTA, 0.3 mM Na-GTP, 2 mM Mg-ATP, 5 mM QX314, 0.5% biocytin (pH 7.2, 280 mOsm/l). The calculated reversal potential for Cl-mediated PSPs (E_{Cl}) for this solution was –20 mV. During mapping, the cell was held at –70 mV. Amplitudes of postsynaptic potentials varied widely between cells, even in the same age group, perhaps due to the large differences in input resistance of immature LSO neurons[29] (**Supplementary Methods**). Recordings were corrected for a liquid junction potential of –7 mV. Data were filtered at 1 kHz (Bessel filter, Axoclamp-1D, Axon Instruments, Foster City, California), digitized at 5 kHz and stored on a computer using custom-written LabView 5.0 software (National Instruments, Austin, Texas).

Recordings in electrical stimulation experiments were made in voltage-clamp using patch electrodes (3–4 MΩ, coated with epoxy, Elementis Performance Polymers, New Jersey) filled with solution containing 54 mM D-gluconic acid, 54 mM CsOH, 56 mM CsCl, 1 mM $MgCl_2$, 1 mM $CaCl_2$, 10 mM Hepes, 11 mM EGTA, 0.3 mM Na-GTP, 2 mM Mg-ATP, 5 mM QX314, 0.5% biocytin (pH 7.2, 280 mOsm/l). In some experiments, the pipette solution additionally contained 0.1 mM D600 (Sigma), an L-type calcium channel antagonist. Series resistance of 5–20 MΩ was compensated by 70–90% (Axopatch-1D) and was continuously monitored throughout recordings. LSO inputs were stimulated by positioning a low-resistance patch electrode (~2 MΩ, filled with artificial CSF) at the lateral end of the MNTB. Electrical stimuli were delivered at a rate of 0.033–0.067 Hz (Master 8 and Isoflex, AMPI, Israel).

During stimulus–response experiments, responses were considered to be maximal if further increase in stimulus intensities led to a decline in response amplitudes or if the responses remained unchanged over about 100 μA (**Supplementary Methods**).

For some experiments, cells were held at +30 mV (**Fig. 6**). In these cells, the quality of voltage control was confirmed by the presence of linear current–voltage relationships ($r = 0.98$) and average reversal potentials of –14.8 ± 0.76 mV ($n = 4$), which is close to the theoretical value (–20 mV). Analysis of electrophysiological data and statistical tests were performed with custom-written LabView 5.0 and Matlab 6.0 (Mathworks, Natick, Massachusetts) programs.

Functional mapping. The spatial distribution of presynaptic MNTB neurons was determined using focal photolysis of *p*-hydroxyphenacylglutamate (150–200 μM)[23,49]. The optical fiber for delivering UV light (duration 50–100 ms) had a 20 μm diameter light-conducting core (Polymicro Technologies, Phoenix, Arizona) that produced almost circular UV spots (diameter ~25 μm) on the surface of the slice. For mapping, the microscope objective was switched to 4×, and 80–100 locations spaced ~45 μm apart, in and around the MNTB, were stimulated (**Fig. 1b**). The location of the light spot on the slice was monitored with a CCD camera and guided by a grid placed on the video monitor. Grid size was ~45 μm, and the same grid was used in all experiments. Accuracy of fiber placement was estimated to be ±10 μm. The location of each recorded LSO neuron and of each MNTB stimulation site was recorded. Consistency of input maps was confirmed by rescanning in about half of the cases. Only one map was obtained per MNTB.

Spatial resolution of uncaging was determined by recording responses of MNTB neurons in current clamp. 'Spike-eliciting distance' to an MNTB cell body was measured between the recording electrode tip and a line drawn between the farthest spike-eliciting light spot and the first subthreshold spot. While mapping subthreshold stimulation areas, the ability of the recorded neurons to generate spikes was confirmed by injecting suprathreshold positive currents after testing each stimulation site.

We found no evidence that uncaging of glutamate activates polysynaptic MNTB–LSO pathways that could increase input areas in young animals. First, MNTB-evoked calcium responses in Fura-2 stained slices were only occasionally observed outside the LSO, despite strong responses in the LSO (**Supplementary Fig. 1**). Second, mapping of intrinsic connections in the MNTB (**Fig. 4**) and LSO (**Supplementary Fig. 2**) revealed no intrinsic connections in these nuclei. These results, together with previous anatomical studies[25], argue against the possibility that the larger input maps in neonatal animals reflect transient polysynaptic pathways between the MNTB and LSO.

Construction and analysis of MNTB–LSO input maps. For each map, stimulation sites were marked by circles aligned to the center of each uncaging site (Adobe Photoshop; **Figs. 1c** and **2**). Peak PSP amplitudes of corresponding PSPs elicited from each site were determined. For each LSO neuron, peak amplitudes were normalized to the largest response (**Fig. 2**). Each successful stimulation site was assigned a filled circle (diameter ~50 μm), and the total area covered by all filled circles was defined as the input area.

To normalize input areas to MNTB cross-sectional areas, MNTB boundaries were determined by three investigators (two of them were blind to the actual data) using video images taken from the slice. MNTB areas determined by the three independent observers were in close agreement (coefficient of variation, 9%), and the mean area was used for normalizing input maps. The width of input maps along the mediolateral MNTB axis was determined by measuring the width of each horizontal row of stimulation sites and calculating the mean width of all rows.

Cluster analysis. To achieve an objective estimate of the number of steps present in the stimulus–response curves, cluster analysis was used on PSC peak amplitudes (partitioning around medoids; S-Plus 2000, MathSoft). This method uses an optimization algorithm in which a sum of dissimilarities is minimized through iterations of grouping. Numbers of suspected clusters for each sequence of iterations were assigned values from 1 to 25. After clustering, an optimal number of clusters was chosen by calculating the silhouette index[50]. In neurons from neonatal animals, any number of potential clusters tested resulted in an equally low silhouette index, indicating the absence of identifiable clusters.

Minimal stimulation. Electrical stimulus intensity was adjusted to give a failure rate of >50% (10–60 μA). At this intensity, 100–300 responses were evoked at 0.03–0.1 Hz. Identification of successful responses and failures was performed offline by eye. Only responses that had latencies that fell within a 1-ms window were accepted, and the mean peak amplitude of those selected minimal PSCs was taken as the size of single-fiber inputs for the cell. As minimal stimulation cannot distinguish whether a given failure is due to a failure in neurotransmitter release or a failure in fiber excitation, all failures were excluded when calculating mean peak amplitudes. Therefore, at all ages, estimated single-fiber response amplitudes are probably biased toward higher values.

Statistical significance. Student's *t*-tests and Kolmogorov-Smirnov tests were used. Data are expressed as mean ± standard error of the mean (s.e.m.) throughout the text.

Note: Supplementary information is available on the Nature Neuroscience website.

Acknowledgments

We thank N.K. Baba, E. Frank, D. Gillespie, E. Rubel and D. Simons for discussions and comments on the manuscript, I. Ehrlich for determining MNTB boundaries and N. Allman for technical support. We are also grateful to R. Givens for php-glutamate and to B. Schmidt for BC204 GABA. This work was supported by the National Institute on Deafness and Other Communicative Disorders (DC04199), the Alfred P. Sloan foundation, a Presidential Early Career Award (K.K.) and the Center for Neural Basis of Cognition (G.K.).

Competing interests statement

The authors declare that they have no competing financial interests.

RECEIVED 20 NOVEMBER 2002; ACCEPTED 23 JANUARY 2003

1. Purves, D. & Lichtman, J.W. *Principles of Neural Development* (Sinauer Associates Inc., Sunderland, 1985).
2. Lichtman, J.W. & Colman, H. Synapse elimination and indelible memory. *Neuron* **25**, 269–278 (2000).
3. Goodman, C.S. & Shatz, C.J. Developmental mechanisms that generate precise patterns of neuronal connectivity. *Cell* **72** (Suppl.), 77–98 (1993).
4. Jackson, H. & Parks, T.N. Functional synapse elimination in the developing avian cochlear nucleus with simultaneous reduction in cochlear nerve axon branching. *J. Neurosci.* **2**, 1736–1743 (1982).
5. Chen, C. & Regehr, W.G. Developmental remodeling of the retinogeniculate synapse. *Neuron* **28**, 955–966 (2000).
6. Stellwagen, D. & Shatz, C.J. An instructive role for retinal waves in the development of retinogeniculate connectivity. *Neuron* **33**, 357–367 (2002).
7. Hubel, D.H., Wiesel, T.N. & LeVay, S. Plasticity of ocular dominance columns in monkey striate cortex. *Philos. Trans. R. Soc. Lond. B Biol. Sci.* **278**, 377–409 (1977).
8. Kilman, V., van Rossum, M.C. & Turrigiano, G.G. Activity deprivation reduces miniature IPSC amplitude by decreasing the number of postsynaptic $GABA_A$ receptors clustered at neocortical synapses. *J. Neurosci.* **22**, 1328–1337 (2002).
9. Rico, B., Xu, B. & Reichardt, L.F. TrkB receptor signaling is required for establishment of GABAergic synapses in the cerebellum. *Nat. Neurosci.* **5**, 225–233 (2002).
10. Hendry, S.H. & Jones, E.G. Reduction in number of immunostained GABAergic neurons in deprived-eye dominance columns of monkey area 17. *Nature* **320**, 750–753 (1986).
11. Hensch, T.K. *et al.* Local GABA circuit control of experience-dependent plasticity in developing visual cortex. *Science* **282**, 1504–1508 (1998).
12. Huang, Z.J. *et al.* BDNF regulates the maturation of inhibition and the critical period of plasticity in mouse visual cortex. *Cell* **98**, 739–755 (1999).
13. Rozas, C. *et al.* Developmental inhibitory gate controls the relay of activity to the superficial layers of the visual cortex. *J. Neurosci.* **21**, 6791–6801 (2001).
14. Knudsen, E.I. Instructed learning in the auditory localization pathway of the barn owl. *Nature* **417**, 322–328 (2002).
15. Kapfer, C., Seidl, A.H., Schweizer, H. & Grothe, B. Experience-dependent refinement of inhibitory inputs to auditory coincidence-detector neurons. *Nat. Neurosci.* **5**, 247–253 (2002).
16. Sanes, D.H. & Friauf, E. Development and influence of inhibition in the lateral superior olivary nucleus. *Hear. Res.* **147**, 46–58 (2000).
17. Rietzel, H.J. & Friauf, E. Neuron types in the rat lateral superior olive and developmental changes in the complexity of their dendritic arbors. *J. Comp. Neurol.* **390**, 20–40 (1998).
18. Sanes, D.H. & Siverls, V. Development and specificity of inhibitory terminal arborizations in the central nervous system. *J. Neurobiol.* **22**, 837–854 (1991).
19. Kotak, V.C., Korada, S., Schwartz, I.R. & Sanes, D.H. A developmental shift from GABAergic to glycinergic transmission in the central auditory system. *J. Neurosci.* **18**, 4646–4655 (1998).
20. Boudreau, J.C. & Tsuchitani, C. Binaural interaction in the cat superior olive S segment. *J. Neurophysiol.* **31**, 442–454 (1968).
21. Irvine, D.R.F. The mammalian auditory pathway: neurophysiology. in *Springer Handbook of Auditory Research* Vol. 2 (eds. Fay, R.R. & Popper, A.A.) 153–231 (Springer-Verlag, 1992).
22. Helfert, R.H. & Schwartz, I.R. Morphological evidence for the existence of multiple neuronal classes in the cat lateral superior olivary nucleus. *J. Comp. Neurol.* **244**, 533–549 (1986).
23. Kandler, K., Givens, R.S. & Katz, L.C. in *Imaging Neurons* (eds. Yuste, R., Lanni, F. & Konnerth, A.) 271–279 (Cold Spring Harbor Laboratory Press, 1998).
24. Kullmann, P.H., Ene, F.A. & Kandler, K. Glycinergic and GABAergic calcium responses in the developing lateral superior olive. *Eur. J. Neurosci.* **15**, 1093–1104 (2002).
25. Lohmann, C., Ilic, V. & Friauf, E. Development of a topographically organized auditory network in slice culture is calcium dependent. *J. Neurobiol.* **34**, 97–112 (1998).
26. Friauf, E. Tonotopic order in the adult and developing auditory system of the rat as shown by c-fos immunocytochemistry. *Eur. J. Neurosci.* **4**, 798–812 (1992).
27. von Gersdorff, H. & Borst, J.G. Short-term plasticity at the calyx of Held. *Nat. Rev. Neurosci.* **3**, 53–64 (2002).
28. Sanes, D.H. The development of synaptic function and integration in the central auditory system. *J. Neurosci.* **13**, 2627–2637 (1993).
29. Kandler, K. & Ecki, F. Development of electrical membrane properties and discharge characteristics of superior olivary complex neurons in fetal and postnatal rats. *Eur. J. Neurosci.* **7**, 1773–1790 (1995).
30. Stevens, C.F. & Wang, Y. Changes in reliability of synaptic function as a mechanism for plasticity. *Nature* **371**, 704–707 (1994).
31. Jonas, P., Bischofberger, J. & Sandkuhler, J. Co-release of two fast neurotransmitters at a central synapse. *Science* **281**, 419–424 (1998).
32. Blatchley, B.J., Cooper, W.A. & Coleman, J.R. Development of auditory brainstem response to tone pip stimuli in the rat. *Brain Res.* **429**, 75–84 (1987).
33. Colman, H., Nabekura, J. & Lichtman, J.W. Alterations in synaptic strength preceding axon withdrawal. *Science* **275**, 356–361 (1997).
34. Antonini, A. & Stryker, M.P. Rapid remodeling of axonal arbors in the visual cortex. *Science* **260**, 1819–1821 (1993).
35. Kandler, K. & Friauf, E. Development of glycinergic and glutamatergic synaptic transmission in the auditory brainstem of perinatal rats. *J. Neurosci.* **15**, 6890–6904 (1995).
36. Ehrlich, I., Lohrke, S. & Friauf, E. Shift from depolarizing to hyperpolarizing glycine action in rat auditory neurones is due to age-dependent Cl^- regulation. *J. Physiol.* **520**, 121–137 (1999).
37. Ben Ari, Y. Developing networks play a similar melody. *Trends Neurosci.* **24**, 353–360 (2001).
38. Kotak, V.C. & Sanes, D.H. Long-lasting inhibitory synaptic depression is age- and calcium- dependent. *J. Neurosci.* **20**, 5820–5826 (2000).
39. Aizenman, C.D., Manis, P.B. & Linden, D.J. Polarity of long-term synaptic gain change is related to postsynaptic spike firing at a cerebellar inhibitory synapse. *Neuron* **21**, 827–835 (1998).
40. Katz, L.C. & Shatz, C.J. Synaptic activity and the construction of cortical circuits. *Science* **274**, 1133–1138 (1996).
41. Kotak, V.C. & Sanes, D.H. Developmental influence of glycinergic transmission: regulation of NMDA receptor–mediated EPSPs. *J. Neurosci.* **16**, 1836–1843 (1996).
42. Kirsch, J. & Betz, H. Glycine-receptor activation is required for receptor clustering in spinal neurons. *Nature* **392**, 717–720 (1998).
43. Sanes, D.H. & Takacs, C. Activity-dependent refinement of inhibitory connections. *Eur. J. Neurosci.* **5**, 570–574 (1993).
44. Gubellini, P., Ben Ari, Y. & Gaiarsa, J.L. Activity- and age-dependent GABAergic synaptic plasticity in the developing rat hippocampus. *Eur. J. Neurosci.* **14**, 1937–1946 (2001).
45. Takahashi, T., Momiyama, A., Hirai, K., Hishinuma, F. & Akagi, H. Functional correlation of fetal and adult forms of glycine receptors with developmental changes in inhibitory synaptic receptor channels. *Neuron* **9**, 1155–1161 (1992).
46. Bormann, J., Hamill, O.P. & Sakmann, B. Mechanism of anion permeation through channels gated by glycine and τ-aminobutyric acid in mouse cultured spinal neurones. *J. Physiol.* (*Lond.*) **385**, 243–286 (1987).
47. Grantyn, R., Kraszewski, K., Melnick, I., Taschenberger, H. & Warton, S.S. *In vitro* development of vertebrate central synapses. *Perspect. Dev. Neurobiol.* **2**, 387–397 (1995).
48. Davis, G.W. & Goodman, C.S. Synapse-specific control of synaptic efficacy at the terminals of a single neuron. *Nature* **392**, 82–86 (1998).
49. Callaway, E.M. & Katz, L.C. Photostimulation using caged glutamate reveals functional circuitry in living brain slices. *Proc. Natl. Acad. Sci. USA* **90**, 7661–7665 (1993).
50. Kaufman, L. & Rousseeuw, P.J. *Finding Groups in Data: an Introduction to Cluster Analysis* (Wiley, New York, 1990).